JOURNAL OF SOLID STATE CHEMISTRY 75, 41–51 (1988)

Synthesis, Structure, Ionic Conductivity, and Phase Transformation of New Double Chloride Spinel, Li_2CrCl_4

R. KANNO,* Y. TAKEDA, A. MATSUMOTO, AND O. YAMAMOTO

Department of Chemistry, Faculty of Engineering, Mie University, Tsu, 514 Japan

AND R. SUYAMA† AND S. KUME

College of General Education, Osaka University Osaka, 560 Japan

Received August 18, 1987; in revised form December 28, 1987

A new double chloride spinel Li_2CrCl_4 was prepared and characterized by Rietveld X-ray structure refinement, differential thermal analysis, high-temperature X-ray diffraction analysis, and electrical conductivity measurement. The new phase has $C2/c$ symmetry with lattice parameters a = 7.446(1), b = 10.162(2), c = 10.172(1) Å, and γ = 132.11(1)°; its monoclinic (m) unit cell is related to that of the parent cubic spinel (c) according to $a_m \sim \frac{1}{2}^{1/2} a_c$, $b_m \sim a_c$, and $c_m \sim a_c$. The structure is a 1 : 1 ordered type with Cr^{2+} and Li^{2-} ions occupying the octahedral sites. The ordered $CrCl_6$ octahedra elongation caused by the strong cooperative Jahn–Teller effect of d^4 state leads to a lattice deformation from orthorhombic to monoclinic symmetry. The monoclinic phase turned reversibly into the cubic spinel through the two-phase region of 222–305°C. Li_2CrCl_4 showed a high ionic conductivity of 6.3×10^{-2} S cm^{-1} at 400°C, and its ionic conduction is discussed in comparison with other chloride spinels, Li_2MCl_4 (M = Mg, Mn, Fe, Co, Cd).

Introduction

The spinel systems, $Li_{2-2x}M_{1+x}Cl_4$ (M = Mg, V, Mn, Fe Cd) have attracted considerable interest not only because of their high ionic conductivity, particularly apparent at moderate temperature (*1–5*), but also because of the transition from a low to a high ionic conducting state exhibited by gradual displacement of lithium ions (*6, 7*). The chloride spinels are reported to have the inverse structure in which half of the lithium ions are tetrahedrally surrounded by chloride ions and the other half, together with the M^{2+} ions, are distributed statistically over the octahedral sites (*6, 8*). The chloride spinels have a high ionic conductivity of around 0.1 S cm^{-1} at 400°C, the value of which is comparable to or greater than those for the high lithium ion conductors reported previously.

As a part of our work on halide spinels, we recently reported new spinels with distorted structure, Li_2MBr_4 (M = Mg, Mn) (*9*) and Li_2MCl_4 (M = Fe, Co) (*10, 11*). Structural study using the X-ray Rietveld method revealed that the orthorhombic distortion in Li_2MCl_4 (M = Fe, Co) was caused by a 1 : 1 ordering of the Li^+ and M^{2+} ions on the

* To whom correspondence should be addressed.

† Present address: Shinnippon Steel Corp., Central R & D Bureau, R & D Laboratories-1, Materials Research Lab.-1, Kawasaki, Japan.

0022-4596/88 $3.00

octahedral sites such that the lithium ions which occupy the *B* sites lie along the *b*-axis and the metal divalent ions lie along the *a*-axis. Conductivity measurement has shown that the orthorhombic distortion causes a considerable degradation of lithium ionic conduction. The orthorhombic spinel transformed at a high temperature to the cubic spinel which showed particularly high ionic conduction.

No spinel formation has been reported for the $LiCl$–$CrCl_2$ system, while in the $LiCl$–MCl_2 (M = Mg, V, Mn, Fe, Co, Cd) systems, the intermediate compounds such as the spinel structure (*1–11*) and the Suzuki-type phase (*12*) were found and were well characterized. The phase diagram of the $LiCl$–$CrCl_2$ system constructed by Seifert and Klatyk in 1964 (*13*) suggested the existence of intermediate compounds; neither the composition nor the structure, however, has been confirmed. Identification of reaction products was found to be rather difficult partly because their X-ray diffraction pattern are similar to those of reactants, and partly because the strong Jahn–Teller effect of Cr^{2+} ions resulted in structural distortion as described later. Nevertheless, the double chromium chloride containing lithium, if it exists, may have a high ionic conductivity, and its structural distortion which might be caused by the Jahn–Teller effect will be of particular interest from a structural viewpoint.

The purpose of this study is to clarify the intermediate compound in the $LiCl$–$CrCl_2$ system. We assumed the existence of Li_2CrCl_4 by making a structure field map and consequently were able to prove its existence. The structure was determined by an X-ray Rietveld analysis and the phase transition was studied using DTA and high-temperature X-ray diffraction measurements. The monoclinic structure was found to transform to the cubic spinel and successively to a defect NaCl-type structure. The ionic conduction in Li_2CrCl_4 will be discussed in comparison with other chloride spinels.

Experimental

Anhydrous lithium chloride, chromium dichloride, cobalt dichloride, and manganese dichloride were used: LiCl, $CoCl_2$, $CrCl_2$: Nakarai Co., >99% purity; $MnCl_2$: Alfa Products. Reactants were dried carefully under vacuum (~1 Pa) at 300°C; their melting points were in good agreement with reported values. The appropriate quantities of reactants were ground together, pressed into a pellet of 60 MPa in a nitrogen-filled glove box, and heated in an evacuated Pyrex tube at 400°C for 1 week. X-ray diffraction patterns of the powdered samples were obtained using both monochromated Cu$K\alpha$ and Cu$K\beta$ radiation and a scintillation detector. A 7-μm-thick aluminum window covered the sample holder to prevent moisture attack during the measurement.

X-ray powder diffraction data for Rietveld analysis were collected on a polycrystalline sample of Li_2CrCl_4 with Cu$K\alpha$ radiation using a high-power X-ray powder diffractometer (Rigaku RAD 12kW) equipped with a graphite monochromator. The sample was kept under a He atmosphere during measurement. Diffraction data were collected by step scanning over an angular range of $10° \leq 2\theta \leq 100°$ in increments of 0.02° at room temperature.

The structural refinement of X-ray data was performed using the Rietveld analysis computer program RIETAN provided by Izumi (*14*). Reflection positions and intensities were calculated for both Cu$K\alpha_1$ (λ = 1.5405 Å) and Cu$K\alpha_2$ (λ = 1.5443 Å) with a factor of 0.5 applied to the latter's calculated integrated intensities. A pseudo-Voigt profile function was used; the mixing parameter γ was included in the least-squares refinement.

High-temperature phases were examined using a high-temperature X-ray diffractom-

eter. Diffraction patterns were taken in a dry nitrogen atmosphere with silicon powder as internal standard. Differential thermal analysis (DTA) was carried out for samples sealed in evacuated silica glass containers with α-Al_2O_3 as a standard. Heating and cooling rates were 1.5°C/min.

Electrical conductivities of ~0.5 g pressed pellets were measured in the temperature range between room temperature and 500°C in a dry argon gas flow. Blocking electrodes were deposited on both sides of the pellets by evaporating gold. The conductivity was obtained by ac impedance measurement with a HP4800A vector impedance meter over a frequency range of 5 Hz–500 kHz. Resistances were derived by interpretation of the complex impedance plane diagram of the data.

Results and Discussion

1. Structure Field Map of A_2BCl_4 Compounds

Previous studies on double chlorides have clarified six high ionic-conductive compounds with the spinel structure Li_2MCl_4 (M = Mg, V, Mn, Fe, Co, Cd). Interrelating the chloride spinels to other A_2BCl_4 compounds and, further, predicting a new compound having the spinel structure, which is suitable for high ionic conduction, are interesting problems. In Table I are summarized the crystal structures of A_2BCl_4-type metal chlorides reported previously. These compounds can be conveniently grouped into six general structure types. The primary factor that controls the occurrence of a particular structure is the size of A^+ and B^{2+} cations. The structure field map showing radius of cation A^+ versus radius of cation B^{2+} is the best way to interrelate these structures. The structure field map for A_2BCl_4 compound is shown in Fig. 1, where Shannon radii (*33*) are used throughout. Six structure fields are fairly well delineated. The map closely resembles that for oxides (*34*); only the Th_3P_4-type does not occur for the oxides. The field map shows in general that the larger the ionic radius, the higher is the coordination number. The spinel structure can be found only for lithium ion as A^+ cation, while the ionic radius of B^{2+} cation ranges from 0.86 (Mg^{2+}) to 1.09 (Cd^{2+}) Å. This suggests a new spinel chloride with divalent chromium ion (0.94 Å).

TABLE I

CRYSTAL STRUCTURE OF A_2BCl_4-TYPE COMPOUNDS

Compound	Crystal structure	Coordination number		Reference
		A ion	*B* ion	
Li_2MgCl_4				(*8*)
Li_2VCl_4				(*15*)
Li_2CrCl_4	Spinel structure	4, 6	6	This study
Li_2MnCl_4				(*8*)
Li_2FeCl_4				(*8*, *11*)
Li_2CoCl_4				(*10*)
Li_2CdCl_4				(*8*)
Li_2ZnCl_4				(*16*)
Na_2CoCl_4	Olivine structure	6	4	(*16*)
Na_2ZnCl_4				(*16*)
Na_2MnCl_4				(*17*)
Na_2MgCl_4				(*18*)
Na_2FeCl_4	Sr_2PbO_4-type structure	7	6	(*18*)
Na_2CdCl_4				(*18*)
K_2MgCl_4				(*19*)
K_2CrCl_4				(*20*)
Cs_2CrCl_4				(*20*)
Cs_2MnCl_4				(*21*)
Cs_2CdCl_4				(*22*)
Cs_2CaCl_4				(*23*)
Cs_2YbCl_4	K_2NiF_4-type structure	9	6	(*24*)
Rb_2MgCl_4				(*25*)
Rb_2CrCl_4				(*20*)
Rb_2MnCl_4				(*26*)
Rb_2CuCl_4				(*27*)
Rb_2CdCl_4				(*28*)
K_2ZnCl_4				(*29*)
Rb_2ZnCl_4				(*30*)
Rb_2CoCl_4				(*30*)
Cs_2MgCl_4				(*19*)
Cs_2CoCl_4	β-K_2SO_4-type structure	9–10	4	(*31*)
Cs_2CuCl_4				(*27*)
Cs_2ZnCl_4				(*31*)
K_2EuCl_4	Th_3P_4-type structure	8	8	(*32*)
K_2SrCl_4				(*32*)

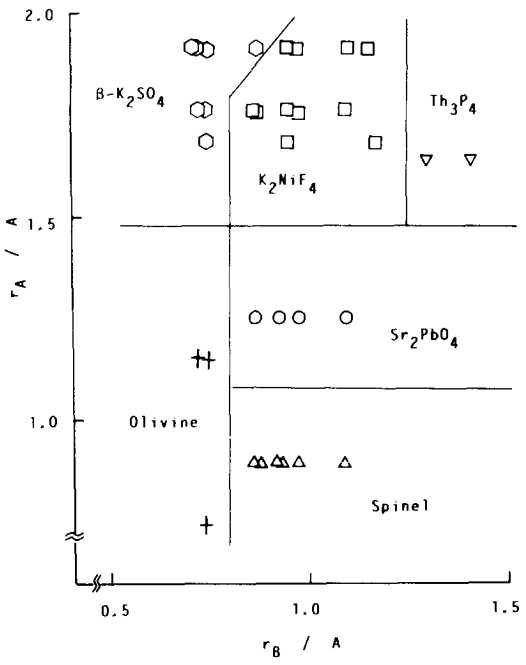

FIG. 1. Structure field map for A_2BCl_4 compounds.

2. *Synthesis and Lattice Distortion*

X-Ray diffraction measurement over the whole composition range in the $LiCl$–$CrCl_2$ system has clarified a new intermediate compound around a composition of 33.3 mole% $CrCl_2$. We thus determined the composition of the new phase by making samples near 33.3 mole% $CrCl_2$ at 2–5 mole% $CrCl_2$ intervals. The intensities of the additional peaks due to LiCl decreased from 10 to 33.3 mole% $CrCl_2$, while in compositions of 36, 38, and 40 mole% $CrCl_2$, the additional X-ray peaks due to $CrCl_2$ were observed. This indicates that the composition of the new phase is Li_2CrCl_4 and that the solid solution represented by $Li_{2-2x}Cr_{1+x}Cl_4$ exists only within a limited range. The X-ray diffraction pattern of Li_2CrCl_4 is similar to that of the orthorhombic spinel Li_2MCl_4 (M = Fe, Co) (*10, 11*); its orthorhombic lattice, caused by a 1 : 1 ordering of the Li^+ and M^{2+} ions on the octahedral sites, was characterized both by the X-ray extra reflections such as $(002)_o$, $(020)_o$, and $(200)_o$ and by the line splitting such that the cubic $(400)_c$ line was split into the orthorhombic $(220)_o$ and $(004)_o$ lines with an intensity ratio of 2 : 1, where the suffixes c and o stand for the cubic and orthorhombic structures, respectively. The similar X-ray peaks of the new chromium spinel Li_2CrCl_4 suggested that the new phase might have a structure closely related to that of the cobalt and iron spinels. However, the distortion of the chromium spinel was apparently large since the line splittings into doublet or triplet in Li_2CrCl_4 could not be indexed by the orthorhombic lattice.

Attempts to prepare single crystals for structure determination were unsuccessful because of a large volume change on sample cooling (see Section 4). We tried to determine the symmetry by making solid solutions with other chloride spinels; continuously shifted X-ray diffraction angles from a known lattice in the solid solution system would facilitate indexing of the line splittings in Li_2CrCl_4.

The solid solution of the Li_2CrCl_4–Li_2MnCl_4 system was first studied. The spinel with manganese divalent ion, next to chromium ion in the first transition metal series, has been reported to have cubic inverse structure. The X-ray diffraction data, however, revealed that the solid solution was formed only within a limited range of $0 < x < 0.1$ and $0.9 < x < 1.0$ in $Li_2(Cr_xMn_{1-x})Cl_4$. The phase diagram constructed by both X-ray diffraction analysis and DTA measurement showed a large miscibility gap.

We thus made the solid solution of the Li_2CrCl_4–Li_2CoCl_4 system; the cobalt spinel Li_2CoCl_4 has the orthorhombic *Imma* cell caused by the cationic ordering on the octahedral sites. The X-ray diffraction measurement on $Li_2(Cr_xCo_{1-x})Cl_4$ revealed monophasic properties with continuously shifted X-ray peaks for the whole range of solid solution. The brief description of the

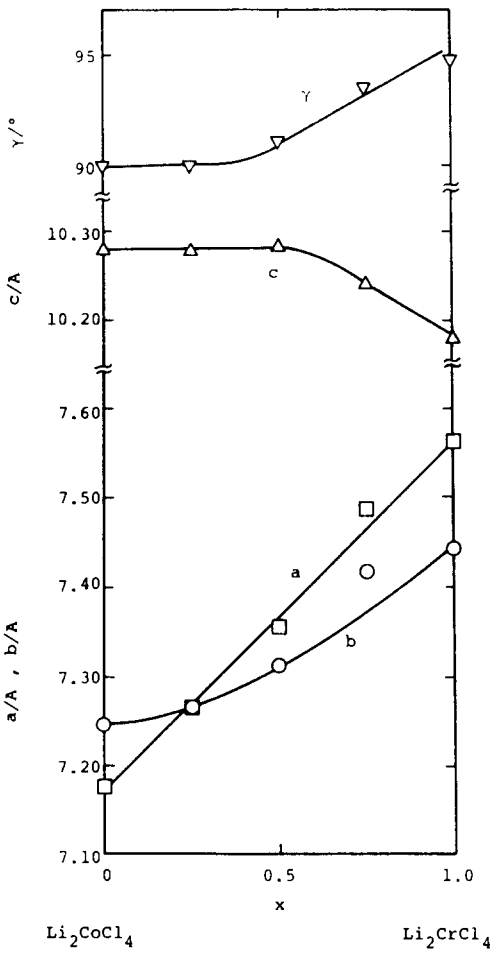

FIG. 2. Lattice parameter change in the $Li_2Cr_xCo_{1-x}Cl_4$ system.

line splittings is as follows. The orthorhombic $(040)_o$, $(224)_o$, and $(400)_o$ lines, derived from the cubic $(440)_c$ line, were resolved into quadruplet. The orthorhombic $(020)_o$ and $(200)_o$ lines, derived from the cubic $(220)_c$ line, shifted into two lines without being split. The orthorhombic $(004)_o$ and $(220)_o$ lines, derived from the cubic $(400)_c$ line, also shifted into two lines. The diffraction pattern of Li_2CrCl_4 was finally found to be indicative of a monoclinic lattice with cell constants, $a = 7.565(4)$, $b = 7.443(4)$, $c = 10.179(8)$ Å, and $\gamma = 94.76(6)°$. Lattice parameter change in the $Li_2Cr_xCo_{1-x}Cl_4$ system is shown in Fig. 2. It is apparent that the distortion increases with decreasing x value. The monoclinic cell (m) with the c-axis setting of "International Tables for X-ray Crystallography" (*35*) was obtained from the above cell (o) derived from *Imma* by the following transformation:

$$\begin{pmatrix} 0 & -1 & 0 \\ 1 & 1 & 0 \\ 0 & 0 & 1 \end{pmatrix} \begin{pmatrix} a_o \\ b_o \\ c_o \end{pmatrix} = \begin{pmatrix} a_m \\ b_m \\ c_m \end{pmatrix}.$$

The new monoclinic cell (m) is related to the parent cubic spinel (c) as follows:

$$\begin{pmatrix} \frac{1}{2} & -\frac{1}{2} & 0 \\ 0 & 1 & 0 \\ 0 & 0 & 1 \end{pmatrix} \begin{pmatrix} a_c \\ b_c \\ c_c \end{pmatrix} = \begin{pmatrix} a_m \\ b_m \\ c_m \end{pmatrix}.$$

The relation among the cubic, orthorhombic, and monoclinic lattice is indicated in Fig. 3. Diffraction extinctions were observed as follows: hkl present only with $k + l = 2n$, $hk0$ only with $h = 2n$ and $k = 2n$, $0kl$ only with $k + l = 2n$, $h0l$ only with $l = 2n$, $h00$ only with $h = 2n$, $0k0$ only with $k = 2n$, and $00l$ only with $l = 2n$. They are characteristic of the space groups $C2/c$ and Cc.

3. *Structural Refinement*

Refinement of the structure proceeded in a straightforward manner with centrosymmetric space group $C2/c$ using the spinel, Li_2CoCl_4, as a model. Initial coordinates were taken as follows: Li(1), $4e(\frac{1}{4}, 0, Z)$ $z \sim -\frac{1}{8}$; Cr, $4d$; Li(2), $4b$; Cl(1), $8f(x, y, z)$ $x \sim$

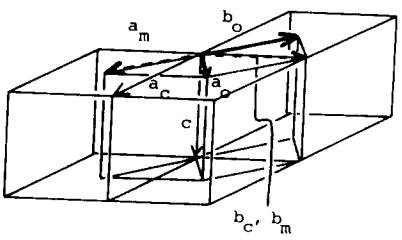

FIG. 3. Relation between the distorted and cubic lattices. The subscripts c, o, and m represent the cubic, orthorhombic, and monoclinic lattices, respectively.

TABLE II

RIETVELD REFINEMENT RESULTS FOR Li_2CrCl_4

Atom	Site	Occupancy	Fractional coordinates			B (Å^2)
			x	y	z	
Li(1)	4e	1	0.25	0	−0.188(23)	15.(10)
Li(2)	4b	1	0	0	0.5	−3.5(24)
Cr	4d	1	0.50	0.25	0.25	0.19(35)
Cl(1)	8f	1	−0.0023(17)	−0.0080(14)	0.258(4)	0.21(43)
Cl(2)	8f	1	0.0018(55)	0.746(6)	0.0073(12)	0.78(37)

0, $y \sim \frac{3}{4}$, $z \sim 0$; Cl(2), 8f $x\sim$, $y \sim 0$, $z \sim \frac{1}{4}$. The refinement was done in stages, with the atomic coordinates and thermal parameters held fixed in the initial calculations and subsequently allowed to vary only after the scale, background, halfwidth, and unit cell parameters were close to convergence to their optimum values. Refinement proceeded to yield agreement factors R_{wp} = 21.96, R_p = 17.52, and R_B = 18.19 with expected agreement R_E = 3.06. Further refinement taking into account the extra conditions, such as a partial disorder of the lithium ions and chromium ions on the octahedral B sites and statistical distribution for lithium ions on the A sites, was not done because of too many parameters for the refinement calculation. Table II shows the final structural parameters for Li_2CrCl_4. The cell parameters are a = 7.446(1), b = 10.162(2), c = 10.172(1) Å, and γ = 132.11(1)°. The interatomic distances and bond angles are listed in Table III.

TABLE III

BOND LENGTHS (Å) AND ANGLES (°) FOR Li_2CrCl_4

Lithium–chlorine octahedron		
Li(2)–Cl(1)	(×2)	2.46(4)[a]
Li(2)–Cl(2)	(×2)	2.49(6)
Li(2)–Cl(2)	(×2)	2.77(3)
Cl(1)–Li(2)–Cl(2)	(×2)	86.7(4)
Cl(2)–Li(2)–Cl(2)	(×2)	88.7(3)
Cl(2)–Li(2)–Cl(2)	(×2)	89.9(15)
Chromium–chlorine octahedron		
Cr(1)–Cl(1)	(×2)	2.778(9)
Cr(1)–Cl(1)	(×2)	2.472(16)
Cr(1)–Cl(2)	(×2)	2.469(12)
Cl(1)–Cr–Cl(1)	(×2)	87.9(4)
Cl(1)–Cr–Cl(2)	(×2)	88.5(11)
Cl(1)–Cr–Cl(2)	(×2)	87.0(18)

[a] The e.s.d.'s presented here are estimates derived from the e.s.d.'s of the atomic coordinates and are merely a guide to the reliability of each value.

The structure of Li_2CrCl_4 derived basically from the inverse spinel structure is isostructural with the orthorhombic spinel, Li_2MCl_4 (M = Fe, Co) and is an ordered type with the chromium and half of the lithium ions occupying the octahedral B sites. The $CrCl_6$ octahedra are connected to each other along ⟨110⟩ direction by sharing Cl(1)–Cl(1) edges, whereas the $LiCl_6$ octahedra are connected along ⟨100⟩ direction. Figure 4 shows a schematic drawing of the lithium and chromium octahedra. The distortion of the $CrCl_6$ octahedra is appreciably large (Cr–Cl: 2.47(×4), 2.78(×2)) and could be induced by the Jahn–Teller instability of Cr^{2+} in the high-spin configuration d^4 state. The octahedra are connected to each other such that the elongated octahedral axis ordered in the same direction. The cooperative Jahn–Teller effect therefore explain the elongation of the $CrCl_6$ octahedra.

The structures and bond distances of the

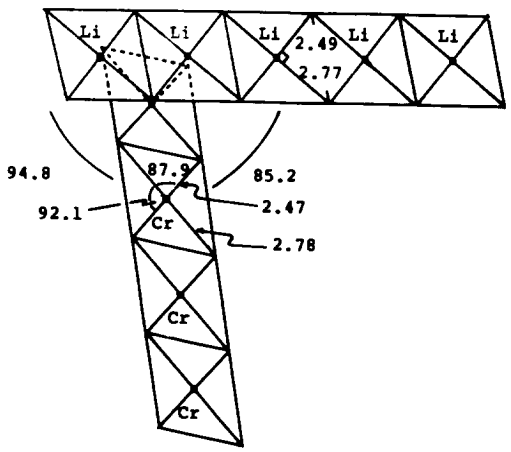

FIG. 4. The structure of Li_2CrCl_4. The rows of lithium and chromium octahedra (qualitative sketch).

chloride spinels are summarized in Table IV. The structures can be classified into two groups, one the cubic spinel and the other the distorted structure; the cubic spinels have inverse nature with random cationic distribution on the octahedral sites, while the distorted spinels are characterized by the 1 : 1 cation order on the octahedral sites. Since the distorted structures are stabilized at room temperature for Cr^{2+}, Fe^{2+}, and Co^{2+} ions having *d*-electron configuration of d^4, d^6, and d^7, respectively, the cooperative Jahn–Teller effect may explain the cationic ordering on the octahedral sites. In addition, difference in ionic radii between M^{2+} and Li^+ may be another reason; the radii of V^{2+}, Mn^{2+}, and Cd^{2+} are larger than those of Fe^{2+} and Co^{2+}, except for Mg^{2+}.

Of these distorted structures, only the chromium spinel has the monoclinic lattice. The rows of Cr octahedra and Li octahedra shown in Fig. 4 are in directions separated by 85.2°, while two rows in the orthorhombic Li_2MCl_4 (M = Fe, Co) are at a right angle to each other (*10, 11*). The ordered Cr Cl_6 octahedra elongation caused by the strong cooperative Jahn–Teller effect of d^4 state gives rise to the lattice deformation from orthorhombic to monoclinic symmetry.

We refined the structure using the models where half of the lithium ions distribute on the tetrahedral *A* sites. However, our previous studies on the orthorhombic Li_2MCl_4 (M = Fe, Co), revealed that in *Imma* the 8i positions placed between the tetrahedral *A* and the interstitial octahedral sites were acceptable for the lithium ions. The same kind of positions might be expected for the lithium ions in Li_2CrCl_4. Further study based on neutron diffraction measurement is nec-

TABLE IV

STRUCTURE AND BOND DISTANCES (Å) IN CHLORIDE SPINELS

M ion	Number of *d*-electron	Symmetry	*M*–Cl distance	*M*–Cl distance (average)	Ionic radii
Mg	0	Cubic	2.523(×6)	2.523	0.86
V	3	Cubic	2.531(×6)	2.531	0.93
Cr	4	Monoclinic	2.472(×2)	2.573	0.94
			2.469(×2)		
			2.778(×2)		
Mn	5	Cubic	2.560(×6)	2.560	0.97
Fe	6	Orthorhombic	2.53 (×4)	2.523	0.92
			2.51 (×2)		
Co	7	Orthorhombic	2.490(×4)	2.487	0.885
			2.481(×2)		
Cd	10	Cubic			1.09

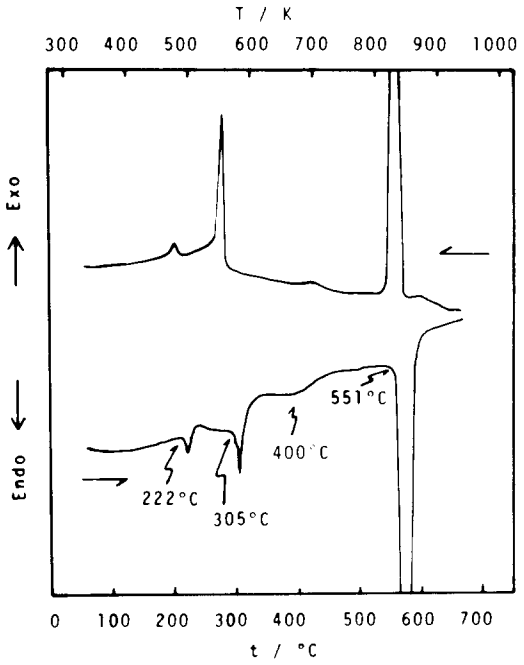

FIG. 5. DTA curves for Li_2CrCl_4.

essary for the purpose of elucidating the lithium position.

4. Thermodynamic Behavior at Elevated Temperatures

Figure 5 shows the DTA curves for Li_2CrCl_4. Three endothermic peaks are clearly observed at 222, 305, and 551°C on heating; the peak at 551°C corresponds to melting. The curves also show a broad endothermic peak near 400°C. High-temperature X-ray diffraction studies were carried out to elucidate phases that appeared at corresponding temperatures. The phases that appeared were determined to be monoclinic spinel for 100 and 200°C, a mixture of the monoclinic and the cubic spinels for 250, 280, and 300°C, and the monophasic cubic spinel for 320°C, this being well consistent with the phase change indicated by DTA at 222 and 305°C. Figure 6 shows thermal evolution of the lattice parameters and volume calculated for the monoclinic spinel, cubic spinel, and defect NaCl-type structures. The phase change through the two-phase region of 222–305°C suggests a certain range of solid solution for both the cubic and monoclinic spinels at higher temperatures. Structurally, the phase change should be considered in relation to the cationic arrangement on the octahedral *B* sites; the ordered arrangement of Li^+ and Cr^{2+} turns reversibly into the disordered state. Large volume difference between the monoclinic and cubic spinels, observed in the two-phase region in Fig. 6, makes it difficult to grow single crystals. Recently, Lutz *et al.* (*36*) reported the existence of

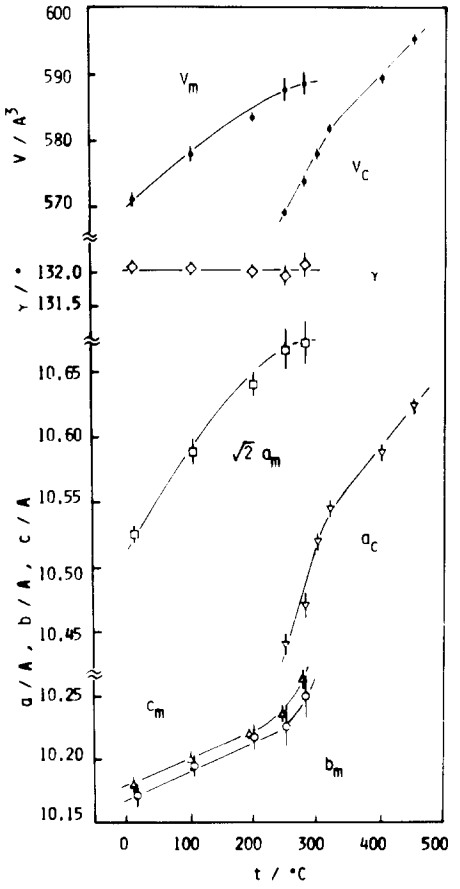

FIG. 6. Thermal evolution of the lattice parameters and volume in the monoclinic spinel, the cubic spinel, and the defect NaCl-type structures.

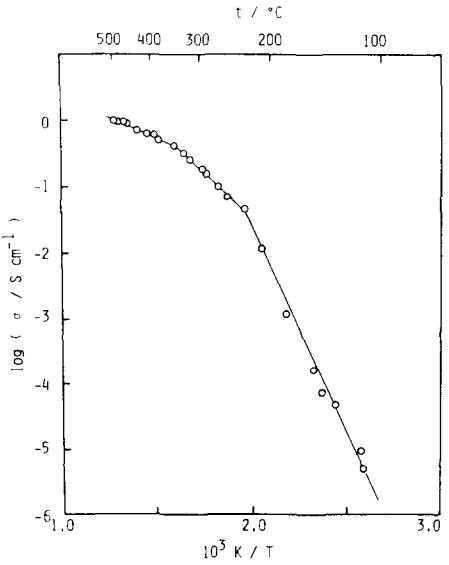

FIG. 7. Thermal evolution of the conductivity for Li_2CrCl_4.

the cubic spinel Li_2CrCl_4 above 314°C, well consistent with our results.

High-temperature X-ray diffraction analysis showed that the intensities of odd numbered lines such as (111) decreased with temperature above 305°C and disappeared around 450°C, this being consistent with the broad DTA peak near 400°C. The results are explained by a transition from the cubic spinel to the defect NaCl-type structure, the precise nature of which was discussed in detail in relation to structural and thermodynamical considerations on $Li_{2-2x}M_{1+x}Cl_4$ (M = Mg, Mn) system (*6, 7*). The transition is concerned with displacement of lithium ions from the tetrahedral 8(a) sites to the interstitial 16(c) sites. In the defect NaCl-type structure, half of the lithium ions is distributed over the octahedral 16(c) sites together with vacancies, while the octahedral 16(d) sites have the same cationic distribution as the spinel structure.

5. *Ionic Conductivity*

Figure 7 shows the Arrhenius plots of the conductivity for Li_2CrCl_4. The chromium spinel showed a high ionic conductivity of 6.3×10^{-2} S cm^{-1} at 400°C, the value of which is comparable to those of other chloride spinels at 400°C. Two distinct breaks in the curve around 230 and 330°C can be explained by the phase change described in the previous section; they correspond respectively to the change from the monoclinic spinel to the two-phase region with the monoclinic and cubic spinels, and to that from the two-phase region to the cubic spinel structure. The activation energies were calculated to be 118 kJ mole^{-1} for the monoclinic spinel (from room temperature to 230°C) and to be 24 kJ mole^{-1} for the cubic spinel (above 330°C). The high-temperature cubic spinel with very low activation energy can be considered as a high ionic conducting phase, which has been found for other halide spinels.

As a part of our work on halide spinels, we reported previously the ionic conductivities of a series of chloride spinels. $Li_{2-2x}M_{1+x}Cl_4$ (M = Mg, Mn, Fe, Co, Cd) (*1, 3, 5, 10, 11*). In Fig. 8 are summarized the activation energies of the stoichiometric chlo-

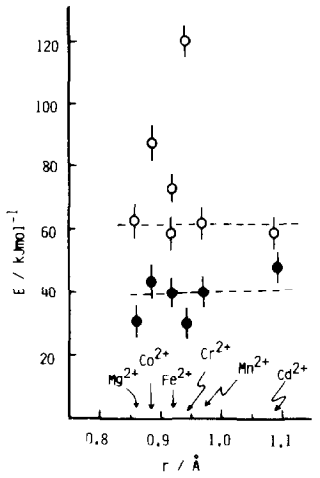

FIG. 8. Activation energies of the chloride spinels as a function of the ionic radii of divalent metal ions. ○, Activation energies at low temperatures; ●, activation energies at high temperatures.

ride spinels Li_2MCl_4 together with Li_2CrCl_4 as a function of ionic radii of metal divalent ions. The activation energies are calculated for both high- and low-temperature ranges, because all spinels showed a break in conductivity curves around 200–300°C. The distorted iron, cobalt, and chromium spinels at lower temperatures have higher activation energies than the cubic spinels, while at higher temperatures, no significant difference was observed. The difference in activation energy between the cubic and distorted spinels was clearly observed in the iron spinel, because two modifications exist in the same temperature range of room temperature to 126°C. The lower ionic conduction for the orthorhombic structure is explained by the differences in both the conduction pathway and the position of the lithium ions (*10, 11*). In the cubic spinel structure, the lithium ions on *A* sites participate in the ionic conduction and the conduction pathway is three dimensional along 8a tetrahedral–16c interstitial octahedral–8a tetrahedral sites (*6*). The ionic conduction of the distorted cobalt and iron spinels, on the other hand, is likely due to a motion of the lithium ions in the 8i sites situated in the octahedron between two tetrahedral *A* sites and the diffusion is one dimensional (*10*). The lower ionic conduction for the monoclinic chromium spinel can also be explained by the conduction mechanism similar to the orthorhombic spinel.

Acknowledgments

Reflection intensity measurements were performed at the Materials Analyzing Center at the Institute of Scientific and Industrial Research, Osaka University. We thank Mr. Tanaka of the Center for his assistance on the measurements. All computations for the structure refinement were carried out at the Crystallographic Research Center, Institute of Protein Research, Osaka University. We thank Professors K. Kamiya and T. Yoko at Mie University for the use of a high-temperature X-ray diffractometer.

References

1. R. KANNO, Y. TAKEDA, AND O. YAMAMOTO, *Mater. Res. Bull.* **16,** 999 (1981).
2. H. D. LUTZ, W. SCHMIDT, AND H. HAEUSELER, *J. Phys. Chem. Solids* **42,** 287 (1981).
3. R. KANNO, Y. TAKEDA, AND O. YAMAMOTO, *Solid State Ionics* **9–10,** 153 (1983).
4. C. CROS, L. HANEBALI, L. LATIE, G. VILLENEUVE, AND WANG GANG, *Solid State Ionics* **9–10,** 139 (1983).
5. R. KANNO, Y. TAKEDA, K. TAKADA, AND O. YAMAMOTO, *J. Electrochem. Soc.* **131,** 469 (1984).
6. J. L. SOUBEYROUX, C. CROS, G. WANG, R. KANNO, AND M. POUCHARD, *Solid State Ionics* **15,** 293 (1985).
7. R. KANNO, Y. TAKEDA, O. YAMAMOTO, C. CROS, G. WANG, AND P. HAGENMULLER, *Solid State Ionics* **20,** 99 (1986).
8. C. J. J. VAN LOON AND J. DE JONG, *Acta Crystallogr. Sect. B* **31,** 2549 (1975).
9. R. KANNO, Y. TAKEDA, O. YAMAMOTO, C. CROS, G. WANG, AND P. HAGENMULLER, *J. Electrochem. Soc.* **133,** 1053 (1986).
10. R. KANNO, Y. TAKEDA, A. TAKAHASHI, O. YAMAMOTO, R. SUYAMA, AND S. KUME, *J. Solid State Chem.* **72,** 363 (1987).
11. R. KANNO, Y. TAKEDA, A. TAKAHASHI, O. YAMAMOTO, R. SUYAMA, AND S. KUME, *J. Solid State Chem.* **71,** 196 (1987).
12. R. KANNO, Y. TAKEDA, A. TAKAHASHI, O. YAMAMOTO, R. SUYAMA, AND M. KOIZUMI, *J. Solid State Chem.* **71,** 189 (1987).
13. VON H.-J. SEIFERT AND K. KLATYK, *Z. Anorg. Allg. Chem.* **334,** 113 (1964).
14. F. IZUMI, *J. Mineral. Soc. Japan* **17,** 37 (1985). [In Japanese]
15. L. HANEBALI, T. MACHEJ, C. CROS, AND P. HAGENMULLER, *Mater. Res. Bull.* **16,** 887 (1981).
16. C. J. J. VAN LOON AND D. VISSER, *Acta Crystallogr. Sect. B* **33,** 188 (1977).
17. J. GOODYEAR, S. A. D. ALI, AND G. A. STEIGMANN, *Acta Crystallogr. Sect. B* **27,** 1672 (1971).
18. C. J. J. VAN LOON AND D. J. W. IJDO, *Acta Crystallogr. Sect. B* **31,** 770 (1975).
19. C. S. GIBBONS, V. C. REINSBOROUGH, AND W. A. WHITLA, *Canad. J. Chem.* **53,** 114 (1975).
20. H.-J. SEIFERT AND K. KLATYK, *Z. Anorg. Allg. Chem.* **334,** 113 (1964).
21. A. EPSTEIN, E. GUREWITZ, J. MAKOVSKY, AND H. SHAKED, *Phys. Rev. B* **2,** 3703 (1970).
22. S. SIEGEL AND E. GEBERT, *Acta Crystallogr.* **17,** 790 (1964).
23. H.-J. SEIFERT AND U. LANDENBACH, *Z. Anorg. Allg. Chem.* **368,** 36 (1969).

24. G. MEYER, *Prog. Solid State Chem.* **14,** 141 (1982).
25. H. T. WITTEVEEN AND J. REEDIJK, *Solid State Commun.* **12,** 397 (1973).
26. J. GOODYEAR, E. M. ALI, AND G. A. STEIGMANN, *Acta Crystallogr. Sect. B* **33,** 2932 (1977).
27. H. T. WITTEVEEN, D. L. JONGEJAN, AND V. BRANDWIJK, *Mater. Res. Bull.* **9,** 345 (1974).
28. H.-J. SEIFERT AND F. W. KOKNAT, *Z. Anorg. Allg. Chem.* **357,** 314 (1968).
29. I. MIKHAIL AND K. PETER, *Acta Crystallogr. Sect. B* **35,** 1200 (1979).
30. S. SAWADA, *Kotaibutsuri* **14,** 51 (1979).
31. B. BREHLER, *Z. Kristallogr.* **109,** 68 (1957); *Kristallografiya* **1,** 291 (1956).
32. H. FINK AND H.-J. SEIFERT, *Z. Anorg. Allg. Chem.* **466,** 87 (1980).
33. R. D. SHANNON AND C. T. PREWITT, *Acta Crystallogr. Sect. B* **25,** 925 (1969); R. D. Shannon, *Acta Crystallogr. Sect. A* **32,** 751 (1976).
34. O. MULLER AND R. ROY, "The Major Ternary Structural Families," Springer-Verlag, Berlin/Heiderberg/New York (1974).
35. "International Tables for X-ray Crystallography," Vol. IV, Knoch Press, Birmingham (1974).
36. H. D. LUTZ, P. KUSKE, AND K. WUSSOW, *Naturwissenschaften* **73,** 623 (1986).